Transitional Modelling of flow over flat plate

Sumedh Soman

Department of Mechanical Engineering, K.J.

Somaiya College of Engineering

Abstract

This report studies the influence of turbulence models and various numerical scheme settings on simulation performance of transitional turbulence over a flat plate. The case chosen was the ERCOFTAC T3A case, and impact of various divergence schemes, solvers, solution algorithms and solver settings on the wall shear stress and turbulent kinetic energy plots was analyzed. Results from the LCTM k-Omega SST model and the standard k-Omega SST model were compared as well. It was concluded that the LCTM k-Omega SST model, coupled with the simpleFoam solver, coupled with the linear upwind divergence scheme and GAMG multigrid solvers provided a blend of high accuracy and relatively lower computational time.

1. Introduction

Transitional turbulence is defined as the process of a flow transitioning from laminar flow to turbulent flow. Transition to turbulence has often been described as proceeding through a series of stages. Depending upon the nature of the flow, the mechanisms governing transition differ. The ERCOFTAC T3A case was chosen to study transitional turbulence over a flat plate. The flow for the given scenario could be construed as a parallel flow. Therefore, the Orr Sommerfeld equation [1], with the help of which it is possible to determine if a perturbation introduced in a parallel, stratified flow will diminish or amplify, can be used to determine whether the flow will transition to turbulence. The equation can be expressed as:

$$(U-c)\left(\phi_{yy}-k^2\phi\right)-U_{yy}\phi=\frac{1}{ik\,Re}\left[\phi_{yyyy}-2k^2\phi_{yy}+k^4\phi\right] \quad (1)$$

This equation cannot be evaluated as it involves 4th order derivatives. Assuming an inviscid flow, which simplifies the equation, it can be seen that stable solutions can only be calculated for a positive value of c. Furthermore, work by Rayleigh showed that for a parallel inviscid flow, a 'point of inflexion' wherein $U_{yy} = 0$ needs to exist for a flow to transition to turbulence. For a Hagen Poiseuille flow case, which is the current flow case being considered, no such inflexion point is present, and therefore the flow remains laminar at high Reynolds numbers, as long as there is no obstacle or adverse pressure gradient. The flat plate acts as an 'obstacle' in this case. Modelling transitional turbulence has always been difficult due to varied mechanisms that govern transition depending upon the flow, and the large number of nonlocal calculations needed, which make implementing transitional turbulence models in modern CFD solvers, which rely on domain decomposition, impossible. The LCTM model [3], which is a modified version of the k-Omega

SST model cures these difficulties. The given model involves solving two convection diffusion equations for intermittency, which is a non-dimensional quantity designed to predict the onset of turbulence and also for transition momentum thickness Reynolds number. The source terms in these equations depend upon empirical correlations created from experimental data. The objective of this report is to study the impact various discretization options and solver settings have on the performance of the LCTM model, as well as a comparison of the results obtained by using the k-Omega SST model and the LCTM model.

2. Problem Statement

Flat plate transitional 2D boundary layer flows with or without pressure gradient, and no temperature variations. Free stream turbulence intensity was set to 3.3% and velocity magnitude equal to 12 m/s in the x direction [4]. Kinematic viscosity was set as 1.5×10^{-5} m^2/s. Details of the experimental setup and the flat plate are shown in the figure below.

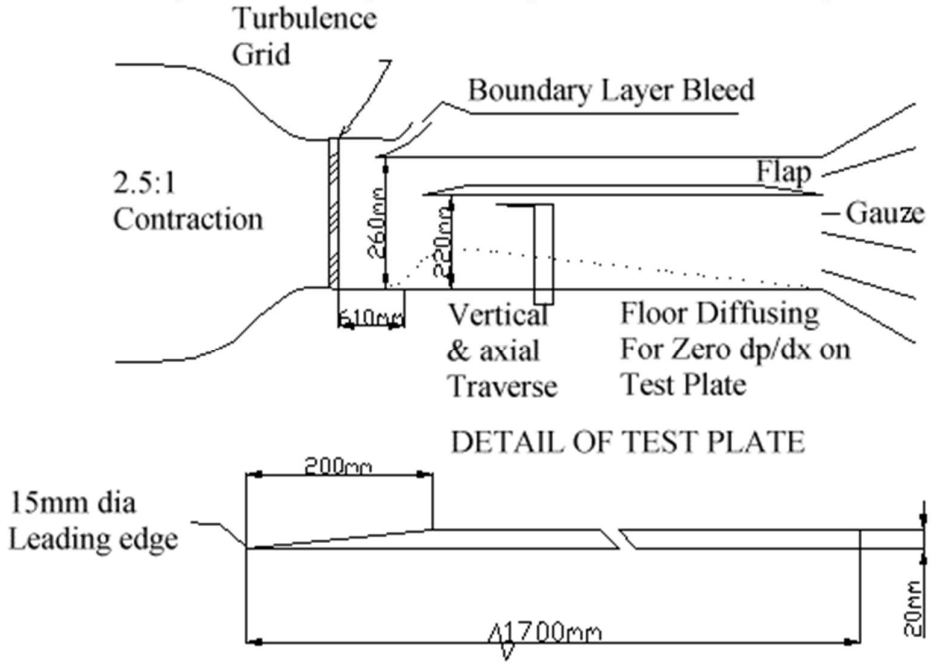

Figure 1: Experimental Setup and test plate details[4]

3. Governing Equations

Two turbulence models were used in the case study, first one being the the k-Omega SST model [2] and second being the LCTM Gamma-Re-Theta model [3]. The equations for the k-Omega SST model are as follows:

$$\frac{\partial(\rho k)}{\partial t} + \frac{\partial(\rho u_j k)}{\partial x_j} = P - \beta^* \rho \omega k + \frac{\partial}{\partial x_j}\left[(\mu + \sigma_k \mu_t)\frac{\partial k}{\partial x_j}\right] \quad (2)$$

$$\begin{aligned} &\frac{\partial(\rho\omega)}{\partial t} + \frac{\partial(\rho u_j \omega)}{\partial x_j} \\ &= \frac{\gamma}{\vartheta_t} P - \beta^* \rho \omega^2 + \frac{\partial}{\partial x_j}\left[(\mu + \sigma_\omega \mu_t)\frac{\partial \omega}{\partial x_j}\right] + 2(1 \\ &- F_1)\frac{\rho \sigma_{\omega 2}}{\omega}\frac{\partial k}{\partial x_j}\frac{\partial \omega}{\partial x_j} \end{aligned} \quad (3)$$

(2) Is a transport equation for the turbulent kinetic energy, and (3) is a transport equation for the specific dissipation.

For the LCTM Gamma-Re-Theta model, two additional transport equations for the intermittency and transition momentum Reynolds number need to be solved, along with a modified version of the k-Omega SST model equations, as mentioned in section 1. The equations for intermittency can be expressed as follows:

$$\frac{\partial(\rho\gamma)}{\partial t} + \frac{\partial(\rho u_j \gamma)}{\partial x_j} = P_\gamma - E_\gamma + \frac{\partial}{\partial x_j}\left[\left(\mu + \frac{\mu_t}{\sigma_f}\right)\frac{\partial \gamma}{\partial x_j}\right] \quad (4)$$

$$P_\gamma = F_{length} c_{a1} \rho S [\gamma F_{onset}]^{0.5} (1 - \gamma) \quad (5)$$

The equation for transition momentum thickness Reynolds Number can be expressed as follows: -

$$\frac{\partial(\rho \overline{Re_{\theta t}})}{\partial t} + \frac{\partial(\rho u_j \overline{Re_{\theta t}})}{\partial x_j} = P_{\theta t} + \frac{\partial}{\partial x_j}\left[\sigma_{\theta t}(\mu + \mu_t)\frac{\partial \overline{Re_{\theta t}}}{\partial x_j}\right] \quad (6)$$

$$P_{\theta t} = c_{\theta t}\frac{\rho}{t}(Re_{\theta t} - \overline{Re_{\theta t}})(1.0 - F_{\theta t}) \quad (7)$$

$$t = \frac{500\mu}{\rho U^2} \quad (8)$$

The equations for turbulent kinetic energy and specific dissipation rate are as follows:

$$\frac{\partial(\rho k)}{\partial t} + \frac{\partial(\rho u_j k)}{\partial x_j} = \tilde{P}_k - \widetilde{D}_k + \frac{\partial}{\partial x_j}\left[(\mu + \sigma_k \mu_t)\frac{\partial k}{\partial x_j}\right] \quad (9)$$

$$\frac{\partial(\rho \omega)}{\partial t} + \frac{\partial(\rho u_j \omega)}{\partial x_j} = \frac{\alpha}{\vartheta_t} P_k - D_\omega + C d_\omega + \frac{\partial}{\partial x_j}\left[(\mu + \sigma_\omega \mu_t)\frac{\partial \omega}{\partial x_j}\right] \quad (10)$$

$$\widetilde{P_k} = \gamma_{eff} P_k \quad (11)$$

$$\mu_t = \left[\frac{\rho k}{\omega}; \frac{a_1 \rho k}{SF_2}\right] \quad (12)$$

4. Simulation Procedure

4.1 Geometry and Mesh

The blockMesh utility was used to generate the mesh for the given case. The geometry has been described in figure 1, accordingly a meshing strategy was formulated, with increased mesh resolution at the leading edge of the plate, since it can be seen from the experimental data that the boundary layer transitions from a laminar to turbulent profile post impact with the leading edge of the plate. The geometry and mesh can be seen as follows:

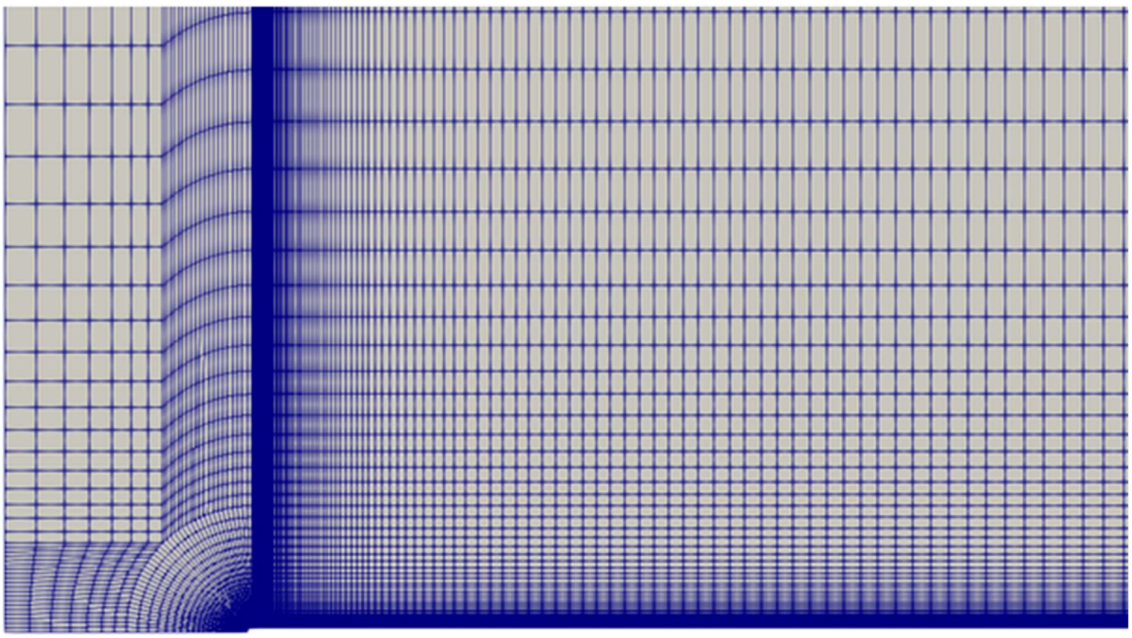

Figure 2: Mesh over the domain

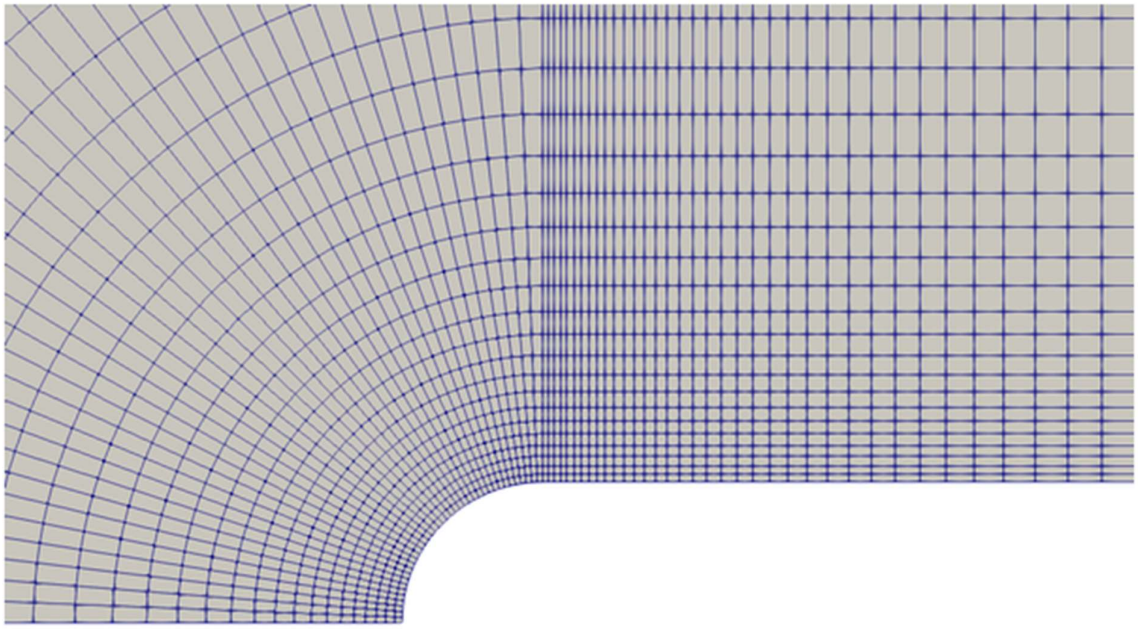

Figure 3: Close up of mesh around the leading edge of the plate

4.2 Initial and Boundary Conditions

The mesh was divided into 5 patches, inlet, outlet, above, top and plate. Front and back were assigned as empty, since the case in consideration is a 2D case. The above and top were designated as slip walls, such that no turbulent kinetic energy production could take place at these walls, only transport of turbulent energy can take place, as the objective is to ensure that the transition process occurs only once the flow hits the leading edge of the plate. The turbulent kinetic energy at the inlet was calculated using the following equation:

$$k_{inlet} = \frac{3}{2}(UI)^2 \tag{13}$$

Where U stands for the velocity and I is the turbulence intensity at the inlet. The specific dissipation rate at the inlet was calculated using the following expression:

$$\omega = \frac{C_\mu^{\frac{3}{4}} k^{\frac{1}{2}}}{l} \tag{14}$$

C_μ is a constant whose value is equal to 0.09, k denotes turbulent kinetic energy, and l is the turbulent length scale.
The plate patch was assigned a no slip condition, with wall functions for turbulent kinetic energy and specific dissipation rate. Since the case is two dimensional in nature, the front and back patches were assigned as empty.

4.3 Divergence Schemes

Divergence schemes approximate the divergence of a given flux. Gauss Divergence Theorem, which links the surface integrals and volume integrals, is used in the process. Three most commonly used divergence schemes are tested, namely linear Upwind, upwind and QUICK

(Quadratic Upstream Interpolation for Convective Kinematics). The upwind divergence scheme sets the flux face value equal to the flux value in the upstream direction. For a single dimension, this can be expressed as [5]:

$$a_P\phi_P = a_W\phi_W + a_E\phi_E \tag{15}$$

Where,

$$a_W = \left(\frac{\Gamma}{dx}\right)_w + \max(\rho u_w, 0) \tag{16}$$

$$a_E = \left(\frac{\Gamma}{dx}\right)_e - \max(-\rho u_e, 0) \tag{17}$$

Where Γ is the diffusivity coefficient.
The Linear upwind scheme is a modification of the upwind scheme, which switches between the Mac Cormack scheme and the upwind differencing scheme via a blending operator ϵ which assumes values of either zero or one. The switching operators are only applied when a local eigenvalue returns a positive value. For a differential equation of the type expressed as-

$$\frac{\partial u}{\partial x} + \frac{\partial F(u)}{\partial t} = 0 \tag{18}$$

The linear Upwind divergence scheme can be expressed as [6]:

$$\begin{aligned} u_j^{i+1} = 0.5\left(u_j^{i+1} + u_j^i\right) - 0.5\frac{\Delta t}{\Delta x}\left[\epsilon_j F_j^n - \left(\epsilon_j - \epsilon_{j-1}\right)F_{j-1}^n + \epsilon_{j-1}F_{j-2}^n\right] \\ - 0.5\frac{\Delta t}{\Delta x}\left[-\epsilon_{j-1}F_{j-1}^{n+1} - \left(\epsilon_j - \epsilon_{j-1} - 1\right)F_j^{n+1} + (1-\epsilon_{j-1})F_{j+1}^{n+1}\right] \end{aligned} \tag{19}$$

Where,

$$\left(\epsilon_j, \epsilon_{j-1}\right) = \begin{cases} (0,0)\ MacCormack\ scheme \\ (0,1)\ MU\ transition\ operator \\ (1,0)\ UM\ transition\ operator \\ (1,1)\ Upwind\ scheme \end{cases} \tag{20}$$

The QUICK scheme is an extension of the upwind scheme. It is expressed, for a 1 D convection-diffusion equation as [7]:

$$a_P\phi_P = a_W\phi_W + a_E\phi_E + a_{WW}\phi_{WW} + a_{EE}\phi_{EE} \tag{21}$$

Where,

$$a_P = a_W + a_E + a_{EE} + a_{WW} + (\rho u_e - \rho u_w) \tag{22}$$

$$a_W = \left(\frac{\Gamma}{dx}\right)_w + 0.75\alpha_w(\rho u_w) + 0.125\alpha_e(\rho u_e) - 0.375(1-\alpha_w)\rho u_w \tag{23}$$

$$a_{WW} = -0.125\alpha_w\rho u_w \tag{24}$$

$$a_E = \left(\frac{\Gamma}{dx}\right)_e - 0.375\alpha_e(\rho u_e) - 0.75\alpha_e(\rho u_e) - 0.125(1-\alpha_w)\rho u_w \tag{25}$$

$$a_{EE} = 0.125(1-\alpha_e)\rho u_e \tag{26}$$

$$\alpha_w > 0\ for\ \rho u_w > 0, \alpha_w < 0\ for\ \rho u_w < 0,\ \alpha_e > 0\ for\ \rho u_e > 0\ and\ \alpha_e < 0\ for\ \rho u_e < 0 \tag{27}$$

4.4 Pressure-Velocity coupling algorithms and solvers

Multiple solver configurations were tested in the given case study. The first approach chosen was using simpleFoam as the pressure velocity coupling algorithm, and using GAMG (multigrid) solvers for pressure and symmetric Gauss Seidel solvers for the remaining variables. Relaxation factor was set as 0.9 for all equations. The second configuration used was simpleFoam with multigrid solvers for all variables, with relaxation factors unchanged. Third configuration employed the same setup as the second configuration, but with different relaxation factors detailed for every field and equation. The fourth and fifth configurations employed pimpleFoam, a transient solver, with solver setups identical to the first and second setup respectively, and changed relaxation factors and residual targets. The first configuration, which is identical to the tutorial configuration for the T3A case present in OpenFOAM documentation [8], was run twice with different residual targets for each run. The solver runtime was set as 1000s, with a timestep of 1s. A summary of various configurations tested and convergence results can be found in Table 1.

Sr. No.	Divergence Scheme	Solver	Pressure Velocity Coupling Algorithm	Relaxation Factors	Convergence	Residual Targets
1	linearUpwind	Pressure: GAMG Rest -GaussSeidel	SIMPLE	0.9 for all equations	Yes, 269 iterations	10^{-5} for pressure, 10^{-6} for velocity, 10^{-4} for other variables
2	upwind	Pressure: GAMG Rest- GaussSeidel	SIMPLE	0.9 for all equations	Yes, 281 Iterations	10^{-5} for pressure, 10^{-6} for velocity, 10^{-4} for other variables
3	QUICK	Pressure: GAMG Rest- GaussSeidel	SIMPLE	0.9 for all equations	No	10^{-5} for pressure, 10^{-6} for velocity, 10^{-4} for other variables
4	linearUpwind	GAMG	SIMPLE	0.9 for all equations	Yes, 193 iterations	10^{-5} for pressure, 10^{-6} for velocity, 10^{-4} for other variables
5	linearUpwind	GAMG	SIMPLE	0.3 for pressure, 0.7 for other variables	No	10^{-5} for pressure, 10^{-6} for velocity, 10^{-4} for other variables
6	linearUpwind	Pressure: GAMG Rest- GaussSeidel	PIMPLE	0.3 for all equations	Solution Diverging	10^{-5} for pressure, 10^{-6} for velocity, 10^{-4} for other variables
7	linearUpwind	GAMG	PIMPLE	0.3 for all equations and 0.8 for final iteration	No	10^{-5} for pressure, 10^{-6} for velocity, 10^{-4} for other variables

As can be seen from Table 1, several configurations and solver settings were tested for the LCTM k-Omega SST Turbulence model. A detailed discussion of each case is presented below:

4.5 Comparison between various divergence schemes

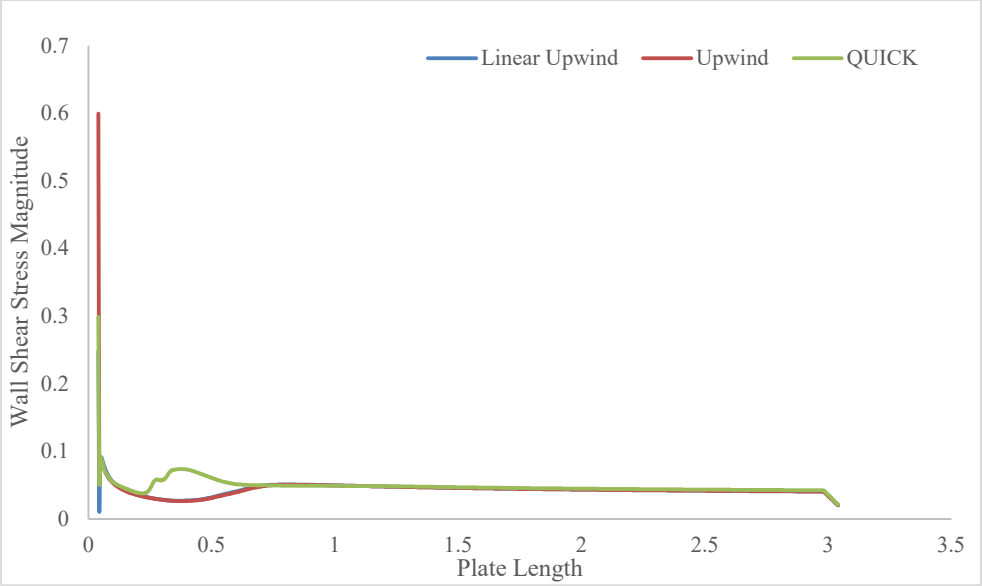

Figure 4: Wall shear stress plots for linear upwind, upwind and QUICK divergence schemes

Figure 4 depicts the variation of Wall shear stress magnitude with respect to the plate length, for three different divergence schemes. It is visible from the plot that the wall shear stress magnitude obtained at the leading edge of the plate is highest for the upwind case, and lowest for the linear upwind case. The overall plots of linear upwind and upwind are quite identical, but the curvature of the plot is noticeably different for the QUICK case. The linear upwind scheme, on many occasions, has proven itself to be the best divergence scheme to be used for bluff body turbulent flows [9] and here too, it can be seen as the scheme with the best performance, with the linear upwind case plots tallying most closely with the experimental values. This can be attributed to the capability of linear upwind to switch between the Mac Cormack and second order upwind scheme, which has proven to reduce spurious oscillations encountered at discontinuities. The upwind scheme also displays the same characteristic curve for the wall shear stress plot as linear upwind, but since it is a first order scheme and also does not have any special provisions for treating discontinuities, we see a significantly higher wall shear stress magnitude at the leading edge of the plate. QUICK was the worst performing scheme of the three; the configuration employing QUICK did not converge even after 1000 iterations; the residuals were oscillating. The QUICK scheme also failed to predict the wall shear stress as accurately as the other two schemes. The lack of convergence can be attributed to the existence of negative coefficients in the scheme, which gives rise to stability problems. Furthermore, QUICK is prone to overshoots and undershoots [10], which might be the reason for the deviation in the wall shear stress plots.

4.6 Comparison between solvers

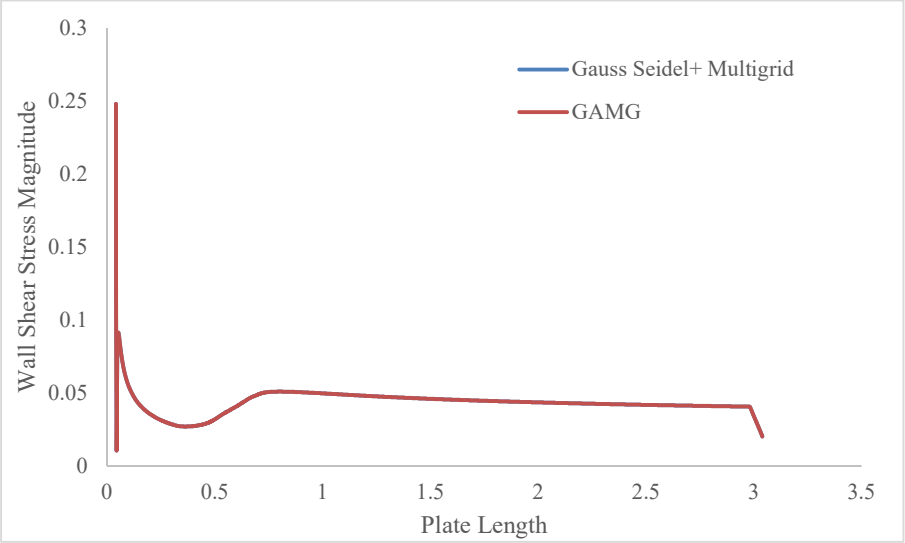

Figure 5: Wall shear stress magnitude plotted against plate length for different solvers

Figure 5 depicts the variation of the wall shear stress magnitude with respect to the plate length, for different solver setups.
It is visible from the plot that the results are identical; there is no noticeable difference in the plots, from which it can be said that the choice of solvers, keeping the relaxation factors same does not impact the output result fields. However, as mentioned in Table 1, the configuration with GAMG solvers converged 71 iterations earlier than the tutorial setup. In any system of equations which are to be solved iteratively, the long wavelength errors decay relatively slowly. The Restriction and prolongation steps employed in the GAMG method, ensure the long wavelength errors are transformed into short wavelength errors which decay quickly, consequently ensuring that the rate of convergence is higher than other solving methods. This mechanism is why a quicker rate of convergence is seen when all variables are solved using multigrid (GAMG) solvers.

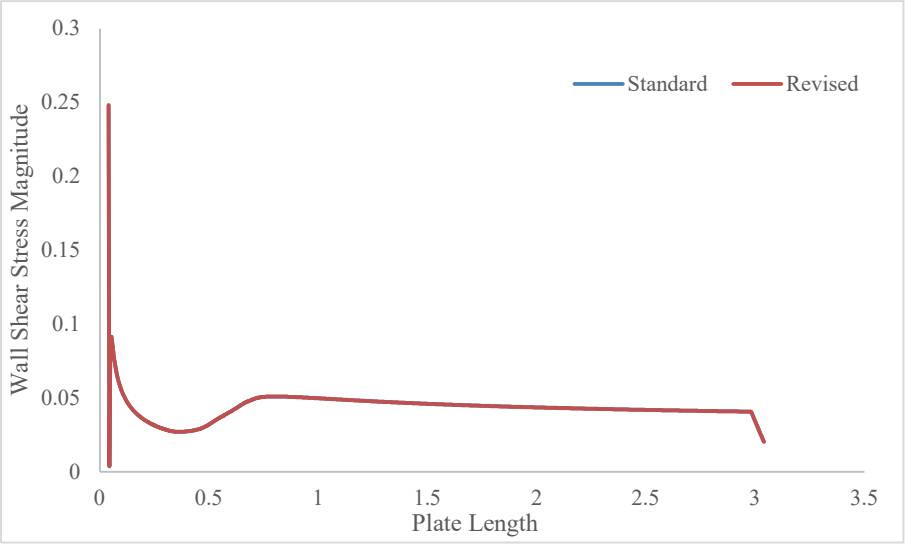

Figure 6: Variance of wall shear stress magnitude with respect to plate length, for two different solver setups with varied relaxation factors

Figure 6 depicts the variation of the wall shear stress magnitude with respect to the plate length, for different solver setups with different relaxation factors. Here, the standard plot depicts the tutorial setup, while the revised plot is with GAMG used for all variables, and a relaxation factor of 0.7 for all equations except pressure field, which was assigned a relaxation coefficient of 0.3. These relaxation factors were chosen from literature [11]. It is observed that the results are identical for the front half of the plate while there is some minute deviation in the rear half of the plate, with the wall shear stress magnitude for the multigrid case being slightly lesser than the tutorial setup.

Also, the solver did not converge even after 1000 iterations, while the tutorial setup converged in 269 iterations. This proves that the original relaxation factors are most appropriate for the given case.

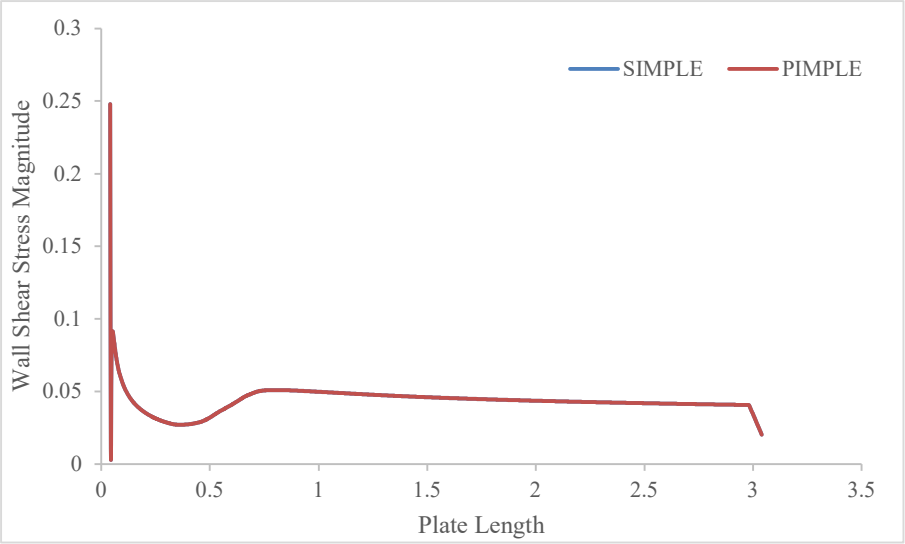

Figure 7: Variance of Wall shear stress along plate length for two different solvers

Figure 7 depicts the variation of the wall shear stress magnitude with respect to the plate length, for different solver setupsS. PimpleFoam is a transient solver; effectively the SIMPLE algorithm is run for every time step. The algorithm is quite tough to stabilize; it has a tendency to diverge quickly. Initial run with multigrid solvers for pressure and Gauss Seidel solvers for other variables began to diverge almost immediately. The second run was with multigrid solvers for all variables and changed relaxation factors, with lower residual targets, the results of which are present in the plot above. The combination of changed relaxation factors and quicker rate of convergence afforded by the multigrid solvers managed to successfully stabilize. Overall, it can be concluded that using PIMPLE is not justified in this case, as the computational cost is too high.

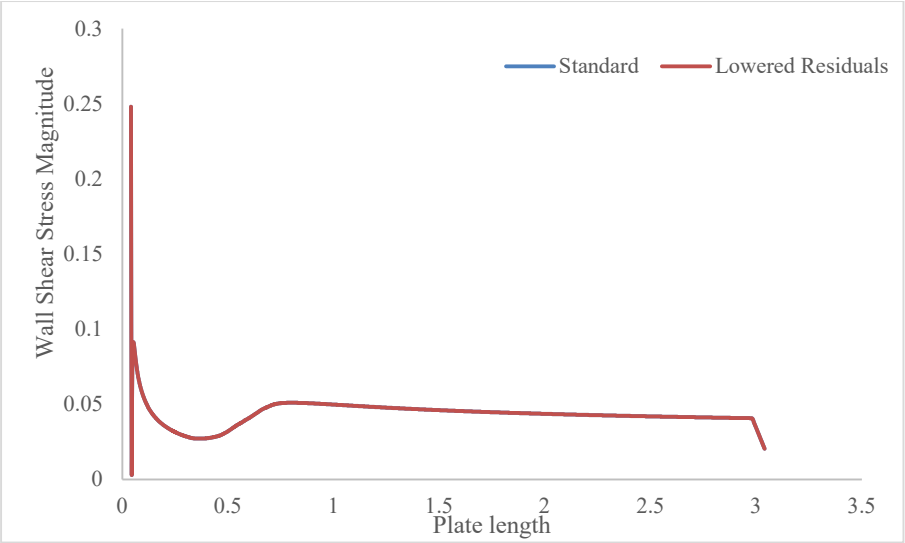

Figure 8: Variance of Wall shear stress along plate length for two different residual values

Figure 8 depicts the variation of the wall shear stress magnitude with respect to the plate length, for different residual targets. It can be observed that there is almost no difference between the two wall shear stress magnitude plots. Also, the run with lower residuals took 361 iterations to converge, so consequently there is no reason to justify the reduced residual targets.

4.7 Comparison between LCTM k-Omega SSTSST and K-Omega SST

To see the exact difference between the standard K-Omega SST and LCTM model predictions, a comparative study was made, with the same solver and discretization settings used (Gauss Linear Upwind was chosen as the divergence scheme, with the GAMG used for pressure and symmetric Gauss Seidel for other variables.

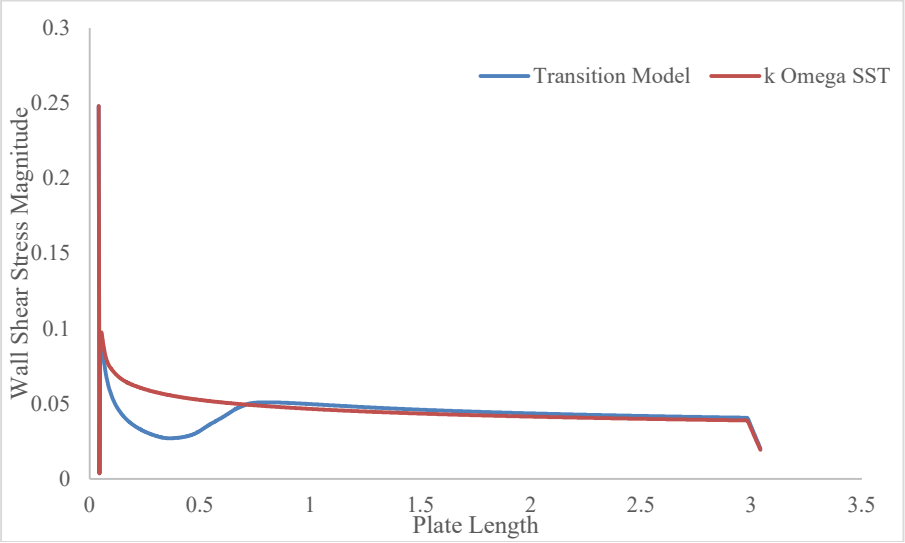

Figure 9: Wall shear stress plotted as a function of plate length for two different turbulence models

Figure 9 depicts the variation of the wall shear stress magnitude with respect to the plate length, for two different turbulence models. It can be inferred from the plots that the transition process was not captured by the K-Omega SST model, wherein the boundary layer momentum thickness first follows a laminar profile, and then the momentum thickness begins to increase as the flow transitions to turbulence. Eventually the boundary layer assumes a fully turbulent profile. Velocity plots around the leading edge of the plate are shown below:-

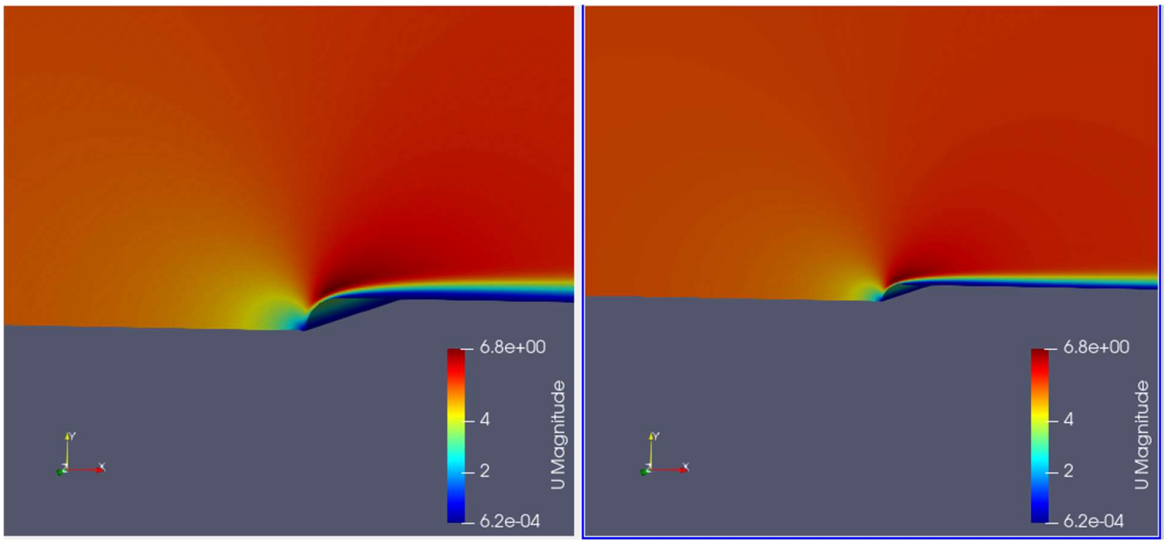

Figure 10: Velocity plot; K-Omega SST plot on the right, and LCTM model plot on the left

It is visible from the above plot that the viscous sublayer is noticeably thicker in the LCTM k-Omega SSTSST plot. This is because the flow is transitioning to turbulence; the boundary layer profile is not fully turbulent at that stage, rather it is closer resembling the laminar boundary layer at that stage.

References

[1] Kundu, Pijush P.; Cohen, M.; Dowling, R.; Chapter 11 - Instability, Editor(s): Pijush K. Kundu, Ira M. Cohen, David R. Dowling, Fluid Mechanics (Sixth Edition), Academic Press, 2016, Pages 533-602, ISBN 9780124059351, https://doi.org/10.1016/B978-0-12-405935-1.00011-3.

[2] Menter, F. R. (1992). Improved two-equation k-omega turbulence models for aerodynamic flows. *Nasa Sti/recon Technical Report N*, *93*, 22809

[3] Menter, F.R., Langtry, R. & Völker, S. Transition Modelling for General Purpose CFD Codes. *Flow Turbulence Combust* **77,** 277–303 (2006). https://doi.org/10.1007/s10494-006-9047-1

[4] Coupland, J. (1990). Ercoftac special interest group on laminar to turbulent transition and retransition: T3a and t3b test cases. *A309514*.

[5] Spalding, D. B. (1972). A novel finite difference formulation for differential expressions involving both first and second derivatives. *International Journal for Numerical Methods in Engineering*, *4*(4), 551-559.

[6] Warming, R. F., & Beam, R. M. (1976). Upwind second-order difference schemes and applications in aerodynamic flows. *AIAA Journal*, *14*(9), 1241-1249.

[7] Leonard, B. P. (1979). A stable and accurate convective modelling procedure based on quadratic upstream interpolation. *Computer methods in applied mechanics and engineering*, *19*(1), 59-98.

[8] OpenFOAM.com, *Turbulence Transition T3A* https://www.openfoam.com/documentation/guides/latest/doc/verification-validation-turbulent-t3a.html

[9] Robertson, E., Choudhury, V., Bhushan, S., & Walters, D. K. (2015). Validation of OpenFOAM numerical methods and turbulence models for incompressible bluff body flows. *Computers & Fluids*, *123*, 122-145.
[10] Versteeg, H. K., & Malalasekera, W. (2007). *An introduction to computational fluid dynamics: The finite volume method*. Harlow, England: Pearson Education Ltd.
[11] Min, C. H., & Tao, W. Q. (2007). An under-relaxation factor control method for accelerating the iteration convergence of flow field simulation. *Engineering Computations*.

.